Electronic Journal of Biotechnology 68 (2024) 11–19

Contents lists available at ScienceDirect

Electronic Journal of Biotechnology

journal homepage: www.elsevier.com/locate/ejbt

Research article

Synthesis of hot spring origin bacterial cell wall polysaccharide-based copper nanoparticles with antibacterial property☆

Aparna Banerjee [a,b], Rajendra Kr Roy [a], Shrabana Sarkar [c], Juan L. López [d,e], Sugunakar Vuree [f], Rajib Bandopadhyay [a,*]

[a] UGC- Center of Advanced Study, Department of Botany, The University of Burdwan, Golapbag, Burdwan 713104, West Bengal, India
[b] Instituto de Ciencias Aplicadas, Facultad de Ingeniería, Universidad Autónoma de Chile, Talca, Chile
[c] Centro de Investigación de Estudios Avanzados del Maule, Vicerrectoría de Investigación y Postgrado, Universidad Católica del Maule, Talca, Chile
[d] Centro de Innovación en Ingeniería Aplicada, Universidad Católica del Maule, Av. San Miguel 3605, Talca, Chile
[e] Centro de Investigación en Ciencias Físico Matemáticas, Facultad de Ciencias Físico Matemáticas, Universidad Autónoma de Nuevo León, Monterrey, Mexico
[f] MNR Foundation for Research & Innovation, MNR University, Sangareddy, India

GRAPHICAL ABSTRACT

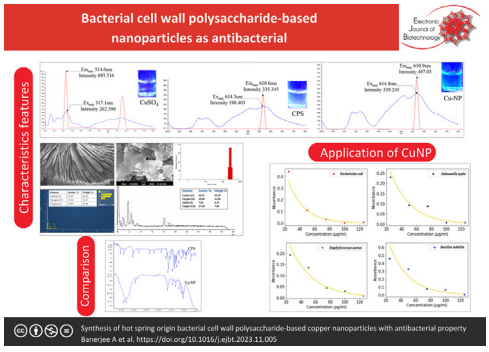

ARTICLE INFO

Article history:
Received 17 May 2023
Accepted 22 November 2023
Available online 23 December 2023

Keywords:
Antibacterial activity
Bacillus
Cell wall polysaccharide
Copper nanoparticles
Green synthesis
Hot spring
Nanoparticles
Thermodynamics
Thermotolerant bacillus

ABSTRACT

Background: At present, research on facile, green synthesis of nanoparticles has significantly increased because of its fast, one-step, cost-effective, time-efficient, and non-toxic nature. In this study, we have reported a single-step green synthesis of copper nanoparticles using cell wall polysaccharides of a hot spring origin, thermotolerant *Bacillus* species.
Result: Copper nanoparticles were characterized using UV-visible spectrophotometry, fluorescence and Fourier transform infrared spectroscopy, scanning electron microscopy with energy dispersive spectroscopy, particle size, and zeta potential analyses. UV-visible spectra of synthesized copper nanoparticles exhibited a band cantered between 220–235 nm, characteristic spectra of copper oxide nanoparticles. Infrared spectra showed the band at 490-530 cm^{-1} corresponding to metal-oxygen or copper nanoparticle vibration, supporting the presence of copper oxide nanoparticles in the monoclinic phase. The energy dispersive spectra of copper nanoparticles exhibited a strong signal from elemental copper. The dynamic Light Scattering pattern confirmed the nanoparticle nature of the studied sample. These nanoparticles showed preferential activity against gram-negative pathogens, *Salmonella typhi* and *Escherichia coli*. The thermodynamic nature of the nanoparticles is also established for its antibacterial actions.

☆ Audio abstract available in Supplementary material.
Peer review under responsibility of Pontificia Universidad Católica de Valparaíso
* Corresponding author.
E-mail address: rajibindia@gmail.com (R. Bandopadhyay).

https://doi.org/10.1016/j.ejbt.2023.11.005

Conclusions: The antibacterial action and its thermodynamics reinforce the possible use of copper nanoparticles as an alternative to commercially available antimicrobials. This study may open a new path for future studies to treat harmful microorganisms resistant to traditional antibiotics in a greener way.
How to cite: Banerjee A, Roy RK, Sarkar S, et al. Synthesis of hot spring origin bacterial cell wall polysaccharide-based copper nanoparticles with antibacterial property. Electron J Biotechnol 2024;68. https://doi.org/10.1016/j.ejbt.2023.11.005.

1. Introduction

Over conventional polysaccharides of plant, algal, and fungal origin, bacterial polysaccharides have advantages as it is usually negative in charge due to the presence of abundant carboxylic and phosphoric functional groups, resulting in electrostatic interactions with positively charged metal ions and organic compounds [1,2]. Bacterial polysaccharides are stable, non-toxic, hydrophilic, and biodegradable polymers [3,4]. Compared to bacterial exopolysaccharides (EPSs), cell wall polysaccharides (CPs) are little explored. CPs are single macromolecules (sacculus) with a minimal two-dimensional polymeric mesh-like structure, which protects the bacterial cell by mechanical strength [5]. Cell wall carbohydrates differ from bacterial EPSs, as bacterial cell wall consists of penicillin-binding proteins (PBPs)-mediated cross-linked peptidoglycan copolymers kept in dynamic shape with the help of hydrolase enzyme [6]. This structural property makes CPs an exciting model for research.

On the other hand, copper (Cu) compounds or Cu ions alone have been used for centuries to disinfect liquids, materials, and human tissue. In 2600 BC, Egyptians mentioned the antimicrobial effect of Cu for the first time. They used Cu powder in wounds and Cu vessels to preserve drinking water, prevent bacterial infection, and destroy parasites and pathogens [7]. The continuous rise in microbial resistance against antibiotics attracts excellent attention toward the antibiotic alternative. Different reports show that many metals and metal oxide nanoparticles (Cu, CuO, Ag, Au, etc.) exhibit broad-spectrum antimicrobial effects by inhibiting the growth of the microorganisms [8,9,10,11]. The chemical or physical nanoparticle (NP) synthesis methods are often toxic and non-ecofriendly. The green synthesis of NPs has attracted researchers' attention for its quick synthesis, cost-effectiveness, eco-friendly and non-toxic nature [12]. NPs are used in various industries due to their unique physicochemical, optoelectronic, and magnetic properties influenced by varied size and shape patterns. In this context, biopolymers are suitable materials for the biogenic synthesis of metal nanoparticles as they function as a capping and stabilizing agent in the synthesis process [13,14]. Thus, CPs may be a potential biopolymer for green NP synthesis with improved activity. The antimicrobial activity of several types of NP depends on the microbial species used for synthesis. For example, the antimicrobial activity of the CuNP was better for *Escherichia coli* (MTCC-441) than for other species [15]. The reports on CuNPs as antibacterial agents are limited compared to the widely used antimicrobials like AgNPs. However, due to their exclusive physicochemical properties, higher stability than AgNPs, and low synthesis cost, CuNP has recently gained scientific interest [16]. If explored more, this can be an essential antimicrobial due to its large surface area and wide range of morphologies [17].

Earlier reports have been on the green synthesis of CuO nanoparticles by *Streptomyces* sp. for developing antimicrobial textiles functional in hospitals to minimize pathogenic bacterial infection [18]. Other than this, CuO nanoparticles are also reported from *E. coli* [19], *Stenotrophomonas*, *Microbacterium* [20] and *Rhodococcus erythropolis* ATCC4277 [21]. CuNPs are extensively used in wound dressings and socks due to their biocidal activity [22,23]. Our study is novel from two aspects: using less explored bacterial CPs instead of other polysaccharides and using Cu with antibacterial properties for CuNP synthesis. For the benefits mentioned above and novelty, this study aims to examine bacterial CPs as biomaterial to synthesize CuNPs, the biocidal property of green synthesized CuNPs for future biotechnological application, and thermodynamic parameters analysis to understand the feasibility and spontaneity of the bioactivity.

2. Materials and methods

2.1. Microorganism

Thermotolerant *Bacillus anthracis* PFAB2 (MCC 3519) has been used for this study. Our group isolated the strain from Panifala hot spring earlier, and it is reported to be a non-pathogenic and exopolysaccharide producer [24]. This strain was cultured in nutrient agar media (Himedia M 001, India) and stored at 4°C. In this study, this bacterial strain has been used to produce CPs.

2.2. Production of bacterial cell wall polysaccharides (CPs)

Three-day-old bacterial culture grown in nutrient broth (HiMedia M 002, India) was centrifuged at 15000 × g, 4°C for 20 min. The pellet was treated with 0.6 M NaCl: 0.06 M of EDTA (10:1) solution at 50°C for 3 h, followed by centrifugation (15,000 × g, 20 min, 4°C). Then, the supernatant vacuum evaporated to half the volume. An equal volume of acetone was treated, and the solution was incubated at –20°C for 72 h. The resulting precipitation was collected by centrifugation (15000 × g, 20 min, 4°C) and washed with chilled acetone a few times. Lastly, CPs were collected and then lyophilized [25], which was used for further experiments.

2.3. Partial characterization of CPs

The surface morphology of lyophilized powder CPs was studied using scanning electron microscopy (SEM) and atomic force microscopy (AFM). For SEM analysis, the CPs were made conductive by gold coating using a Gold Sputter Coater (DII 29030SCTR Smart Coater), and its surface structure was observed under FESEM (JEOl-JSM 7610FPlus) at 15 kV accelerating voltage. The elemental mapping of the CPs was performed using energy dispersive X-ray spectroscopy (EDS) (X-Max AZtec, Oxford Instruments) to analyze carbon/nitrogen/oxygen/phosphorus/sulfur composition. For AFM analysis, a 1 mg ml^{-1} aqueous CP solution was prepared. The stock solution was shaken vigorously in a vortex to dissolve the CPs entirely at room temperature. Approximately, five µl of CP solution was dropped on the surface of a cover glass and dried at room temperature. Finally, the surface images of the CPs were obtained using an AFM (di-INNOVA, Bruker) at the tapping mode of the NanoDrive Innova system.

For thermogravimetry/differential thermal analysis (DTG), the Diamond TG/DTA (Perkin Elmer) instrument was used to deter-

mine the thermal stability of the CPs. TG/DTA thermograms were recorded using ~5 mg CPs in a temperature range of 0–1000°C in a nitrogen atmosphere with a control alumina pan.

2.4. Green synthesis of CPs-mediated CuNPs

Lyophilized CPs as substrate and copper sulfate ($CuSO_4$) (Himedia, India) as precursor were used to synthesize CPs-based CuNPs. The initial concentration of precursor substrate was kept 1:1; *i.e.*, 1 mM $CuSO_4$ was mixed with 1 mM CPs. The synthesis of CuNPs was optimized by varying the concentration to 2:1 (2 mM $CuSO_4$: 1 mM CPs) and 1:2 (1 mM $CuSO_4$: 2 mM CPs). The mixture was incubated at 45°C overnight, and NP formation was detected by observing the color change of the solution. A total of 1 mM CP solution and 1 mM $CuSO_4$ solution were considered respectively as the controls for this experiment [26]. Further, the colloidal NP suspension was centrifuged (10000 × g, 10 min, 4°C), washed, and lyophilized for further usage.

2.5. Characterization of CPs-mediated CuNPs

The change of color of CPs and $CuSO_4$ containing reaction mixture was examined under UV-Vis spectrophotometer (Shimadzu UV-2600) in a wavelength range of 200–800 nm along with two controls. The formation of CuNPs by reducing the Cu ions was confirmed by examining photoluminescence spectra using the PerkinElmer LS 55 fluorescence spectrometer. The role of functional groups present in the structure of CPs that took part in CuNP synthesis was analyzed by Fourier-transformed infrared (FTIR) spectroscopy using PerkinElmer FTIR (model RX1). For FTIR spectroscopic analysis, the sample was pressed against the KBr pellet as per the method described before [27] and scanned in the frequency range of 500–4000 cm^{-1} with a resolution of 1 cm^{-1}.

The microstructure of freshly prepared CuNPs was studied using SEM as characterized before by Laiman et al. [28]. For this, 1 mg of CuNPs were suspended homogenously in 1 ml of deionized water to get the concentration of 1 mg ml^{-1}. One drop of that suspended solution of CuNPs was mounted on the cover glass and made conductive by platinum coating JEOL JFC 1600 Auto Fine Coater. The sample-coated cover glass was observed under JEOL JSM-6390 with an accelerating voltage of 20 kV. The presence of elemental Cu in the freshly prepared CuNPs was analyzed using EDS (INCA 250 EDS). Particle size analysis of CuNP in solution was performed using a Zetasizer instrument (Model Nano ZS, Malvern Instruments Ltd, UK) in UV-grade cuvettes. To determine particle size, 1 mg ml^{-1} NP stock solution was prepared using millipore water, of which 100 µl solution was taken to prepare a working suspension of 10 ml. The zeta potential of the stock solution was recorded using Zetasizer Nano ZS (Malvern Instruments, UK). All measurements were performed in triplicates.

2.6. Antibacterial property elucidation

CuNP solution, along with the control CPs and $CuSO_4$ solutions, was screened for potential *in vitro* antibacterial activities against Gram-positive (*Staphylococcus aureus* NCIM 2122 and *Bacillus subtilis* NCIM 2533) and Gram-negative (*Salmonella typhi* NCIM 2501 and *Escherichia coli* NCIM 2832) bacteria by standard agar cup method on Mueller Hinton agar (Himedia M 173, India) media. Prepared media was poured into sterile Petri plates, and using a sterile cotton swab, microorganisms were spread separately on the agar plate surface, as reported earlier by Adhikari et al. [29]. The experiment used Ampicillin and chloramphenicol (HiMedia) for positive control. A total of 200 µl sample was taken for each synthesized CuNPs (1:1, 2:1, and 1:2), $CuSO_4$, CPs concentration; *viz.* 250, 500, 750 and 1,000 µg ml^{-1}. Treated Petris was incubated at 37°C overnight, and the inhibition zones (mm) against each CuNP were measured.

Minimum inhibitory concentration (MIC) and maximum biocidal concentration (MBC) were checked for the CuNP concentration. The CuNP was serially diluted from 1 to 50 µg ml^{-1}. Each concentration was treated with freshly inoculated microbial cultures in a 1:20 (v/v) ratio. All the treatments were further incubated at 37°C for overnight. A UV–Vis spectrophotometer (Shimadzu UV-2600) was used the next day to record the treatments' absorbance at 595 nm. All the readings were recorded in triplicates.

2.7. Thermodynamic study

The thermodynamic parameters analysis gives information about the feasibility and spontaneity nature of the adsorption process of the CuNPs in the bacterial system [30]. In this sense, the Gibbs free energy change, enthalpy, and entropy can be estimated from the thermodynamic equilibrium state as the following equations [**Equation 1** and **Equation 2**]:

$$\Delta G^i = \Delta H^i - T\Delta S^i \tag{1}$$

$$\ln\frac{C_b}{C_a} = \frac{\Delta S^i}{R} - \frac{\Delta H^i}{RT} \tag{2}$$

Combining the above two equations, the following equations [**Equation 3**, **Equation 4**] are obtained:

$$\Delta G^i = -RT\ln\frac{C_b}{C_a} \tag{3}$$

$$\frac{C_b}{C_a} = e^{-\frac{\Delta G^i}{RT}} \tag{4}$$

where T is the absolute temperature (K), R is the molar gas constant (8.314 J $mol^{-1}K^{-1}$), equilibrium concentrations of the CuNPs were denoted by C_b and C_a in adsorbent and solution (µg ml^{-1}), ΔH^i is adsorption enthalpy change (kJ $mol^{-1}K^{-1}$) and ΔS^i is adsorption entropy change (J $mol^{-1}K^{-1}$).

Positive values of Gibbs free energy change (ΔG^i) indicated the adsorption process is unspontaneous. Positive values of enthalpy change (ΔH^i) indicated that adsorption is a physical and endothermic process, and positive entropy values suggest that the randomness at the solid-liquid interface increased with concentration decrease [31,32]. To estimate the Gibbs free energy change (ΔG^i), it is necessary to study the effect of temperature on the concentration factor $\frac{C_b}{C_a}$ [31,32,33,34]. Furthermore, when the experiments require work at a constant temperature ($T = \text{cte}$), the evaluation is complex. In this work, we address an empirical approach that considers the relationship between $\frac{C_b}{C_a}$ and the absorbance $A(\rho)$ [**Equation 5**]:

$$\frac{C_b}{C_a} = \frac{A(\rho)}{A_0} \tag{5}$$

where ρ is the concentration of CuNPs (µg/ml) and A_0 represents the baseline absorbance (quasi-equilibrium) for any initial ρ concentration, which is characteristic for each particular case.

Likewise, making small changes in the CuNP concentration will allow for achieving a sequence of equilibrium states and, therefore, small Gibbs free energy change (ΔG^i). In this way, we can establish the relationship between the change in Gibbs free energy and the concentration as **[Equation 6 and Equation 7]:**

$$\Delta G^i = f(\rho, T) \tag{6}$$

$$f(\rho,T) = -(\frac{k}{RT})\rho \quad (7)$$

where k (J μg $mol^{-1}ml^{-1}$) is a proportionality factor that expresses the Gibbs free energy change (J mol^{-1}) in response to the CuNP concentration (μg ml^{-1}). In this way, from [**Equation 4**, **Equation 5**, and **Equation 7**] we obtain:

$$A(\rho) = A_0 e^{-(\frac{k}{RT})\rho} \quad (8)$$

3. Results

3.1. Partial Characteristics of CPs

SEM and AFM results were analyzed in detail to study the surface morphology and three-dimensional (3D) alignment of the CPs. This also helped to comprehend the physical properties of CPs, facilitating the understanding of the interaction with Cu to synthesize NPs. As perceived from the acquired SEM images (in 3000×, 5000×, and 10,000× magnifications), CPs produced by thermotolerant *B. anthracis* PFAB2 exhibited characteristic star-shaped flower-like radiant organization with an amorphous surface, which indicates the compact structure of the biopolymer (Fig. 1A, 1B, 1C). AFM analysis showed a similar two-dimensional (2D) amorphous, compact arrangement of the CPs (Fig. 1D). The tapping phase of CPs is composed of unevenly distributed lumps with a three-dimensional (3D) height range of ∼26 nm (Fig. 1E).

The thermal behavior of CPs isolated from thermotolerant *B. anthracis* PFAB2 was analyzed from the DTG study. CPs went through a 7.24% mass loss up to 266.09°C followed by temperature stability at ∼315°C with a characteristic exothermic peak at 246.39°C. The exact degradation temperature (T_d) of the CPs was ∼283.10°C (Fig. 1F).

The 3D layered EDS spectrum showed major elements, carbon, nitrogen, and oxygen, in CPs produced by *B. anthracis* PFAB2 (Fig. S1). The spectrum showed firm peaks for carbon (44.93%) followed by oxygen (38.80%) and nitrogen (16.27%) of total weight. According to atomic weight, the sequence of the elements present in the CPs was also identical, i.e., Carbon (51.05%) > oxygen (33.09%) > nitrogen (15.86%). Little other elements, such as phosphorus and sulfur, were also present (Fig. S1).

3.2. Green synthesis of CPs-mediated CuNPs

The colloidal suspension of CuNPs has been found evident by visually inspecting the solution. The synthesis of CPs-based CuNP was primarily confirmed by the color change of the reaction mixture from colorless to bluish under fluorescence (Fig. 2). The control CPs solution and $CuSO_4$ solution remained colorless, whereas the CPs-$CuSO_4$ solution became bluish, confirming the synthesis of CuNPs. Blue coloration increases with increasing $CuSO_4$ concentration. CPs: $CuSO_4$ (2:1) has shown minor coloration, followed by CPs: $CuSO_4$ (1:1) with the most bluish CPs: $CuSO_4$ (1:2). Among all conditions, the best CuNP synthesis was accomplished at 1:1 (w/w) ratio of precursor and substrate compare two other different ratios of precursor and substrate, which was considered for further experiments.

3.3. Characterization of the CPs-mediated CuNPs

Biogenic synthesis of CuNPs can be confirmed by measuring surface plasmon resonance (SPR) using UV-Vis spectrophotometry. Synthesized nanoparticles exhibit peaks between 220 and 235 nm (Fig. 2A), characteristic spectra for copper oxide NPs due to SPR. Similar SPR was found previously in the case of CuO nanoparticles synthesized from leaf extract of medicinally essential plants, namely *Azadirachta indica, Hibiscus rosa-sinensis, Murraya koenigii on, Moringa oleifera* and *Tamarindus indica* by Rehana et al. [35]. Emission bands have been found around 610 nm (Em_{max}) with a low-intensity peak of 500 nm (Fig. 2C–2E).

FTIR spectra of both CPs and CPs-mediated CuNPs have been represented in Fig. 2B. Shifting of bands observed for CuNPs compared to the control CPs is the characteristic indication of nanoparticle synthesis. A clear peak at 3300 cm^{-1} for primary amine N—H stretching vibration is kept in the case of CuNP but absent in the case of CPs. The 490–530 cm^{-1} peaks showed stretching corresponding to metal-oxygen or CuNP vibration that supports the presence of the monoclinic phase of CuO NPs. It also exhibits a band in the region 3300 cm^{-1} due to primary amine N—H stretch-

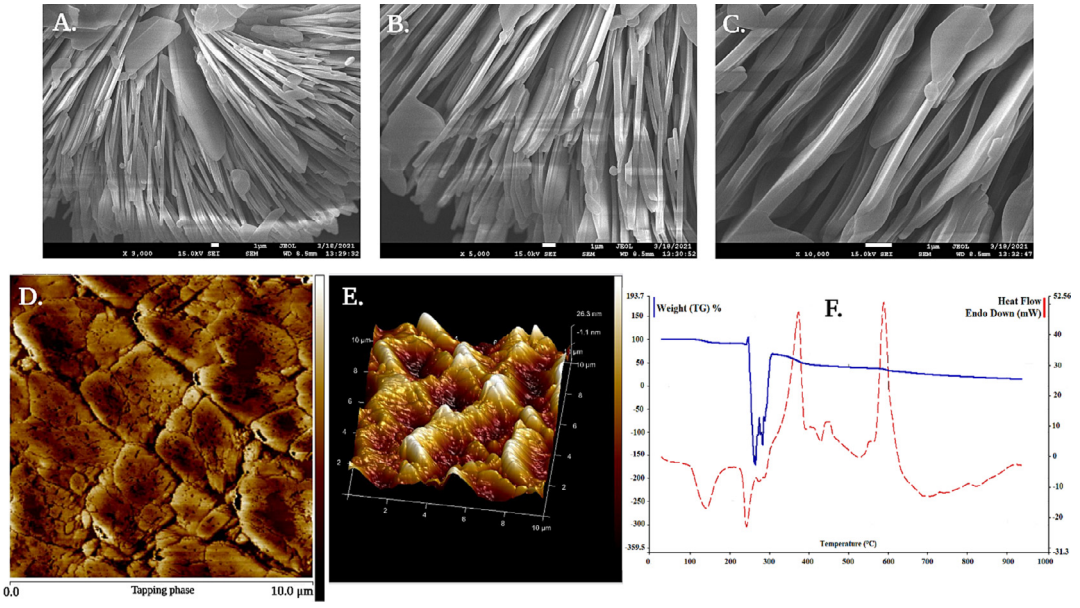

Fig. 1. Surface microstructure determination of the CPs. **(A-C)** SEM images at 3,000×, 5,000×, and 10,000× magnifications; **(D-E)** 2D and 3D surface morphology elucidation by AFM; **(F)** thermal behavior in TG/DTA plot.

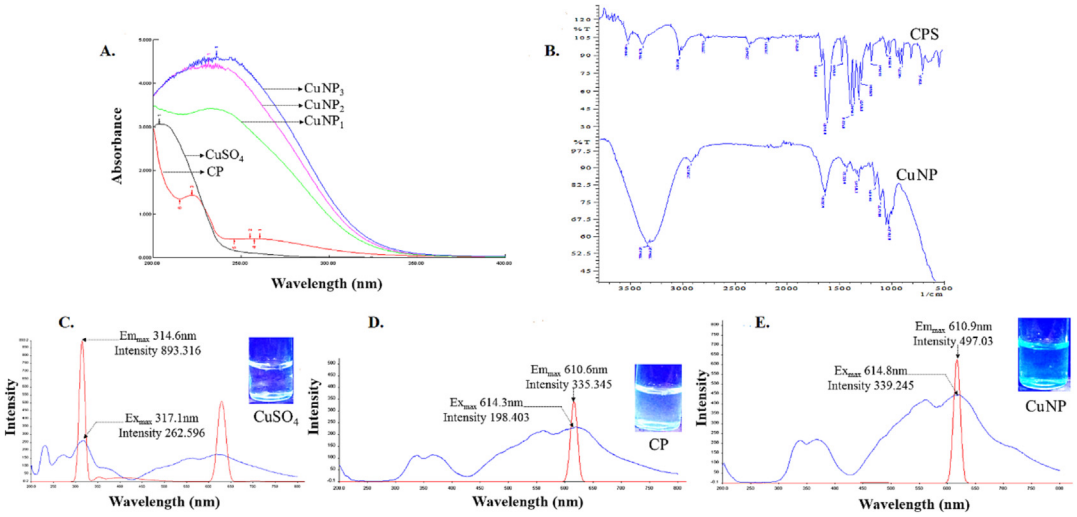

Fig. 2. Characterization of the CPs-based CuNPs. (A) UV–Vis spectrophotometry showing the absorbance peak of CuNP; (**B**) FTIR spectra showing the shifting of functional groups present in the CuNP fabrication (both CPs and CuNP), and Em_{max}, Ex_{max} and Intensity of (**C**) $CuSO_4$ solution, (**D**) CPs solution; (**E**) CPs-based CuNP solution.

ing vibration, whereas the band at ~2900 cm^{-1} is attributed to the intense stretching of C—H groups. The bands around 2100–2300 cm^{-1} are due to variable -C≡C— stretching, whereas that at 1637 cm^{-1} corresponds to the C=C stretching vibration. The characteristic band at 1427 cm^{-1} corresponds to variable C—H bending vibrations. Strong stretching ~1050–1150 cm^{-1} is due to the presence of C—O groups.

SEM is a dynamic equipment to study the morphology of NPs. Green synthesized CuNPs observed at 5,000× and 10,000× magnifications are represented in Fig. 3A, 3B. Scanning micrograph determined the morphology of agglomerated CuNPs embedded in CPs, which is spherical, clustered, and scattered with a rough surface. A similar study was reported before for AgNPs by Rajoka et al. [14], where the shape of the nanoparticle was spherical. The EDS spectrum designated 17.43% of the Cu in synthesized CuNPs. According to the atomic weight, the amount of Cu (27.28%) is found to be higher enough than oxygen (20.69%) and sulfur (7.82%), which is due to the oxidative reduction reaction (Fig. 3C).

The zeta potential value is usually required to understand the interaction between the particles in the suspension [36]. The magnitude (-30mV to + 30mV) of zeta potential define the stability of nanoparticle colloidal suspension [27]. The zeta potential value of *B. anthracis* PFAB2 produced CPs-based CuNP was -3.84 mV. The mean crystalline size of CPs-based CuNPs had a Z-average diameter value of 702.95 nm (Fig. 3D). Polydispersity index (PDI) of synthesized CuNPs was found to be 0.437 (Fig. 3E), which supported that the nanoparticles were polydisperse.

3.4. Antibacterial property elucidation

The antibacterial activity of CPs-based CuNPs has been tested against Gram-positive *S. aureus* and *B. subtilis* and Gram-negative *S. typhi* and *E. coli* by performing an agar cup assay method [37]. The result of the antibacterial activity has been depicted in Fig. S2, where two negative controls (CPs aqueous solution and 1 mM $CuSO_4$ solution) and two positive controls (ampicillin; 10 mcg/disc and chloramphenicol; 30 mcg/disc) were used. The CP suspension has not shown antibacterial activity, whereas the $CuSO_4$ solution has less antibacterial activity than the CuNPs (Fig. S2). The bactericidal activity of the EPS-coated CuNPs was evaluated using the most effective concentration (1:1). From MIC/ MBC analyses, it was observed that the CuNP showed the lowest and most effective antibacterial activity in terms of MIC

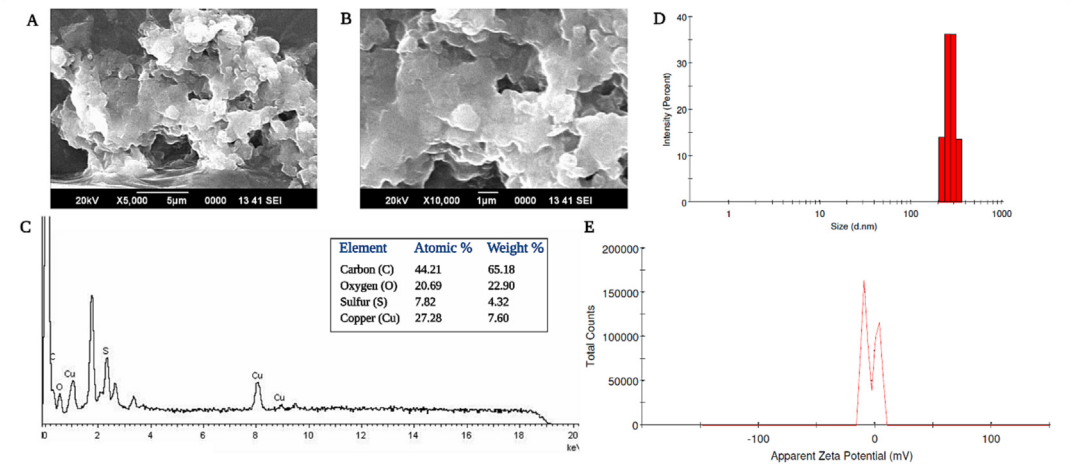

Fig. 3. Microstructure analysis of CPs-based CuNPs. (A) and **(B)** scanning electron microscopic images at 5,000× and 10,000× magnifications, respectively; **(C)** EDS-profile showing the presence of elemental copper in the CuNP solution; (**D**) Size (d.nm) profile; **(E)** Apparent zeta potential distribution profile of bio-fabricated CuNPs.

for gram-negative *S. typhi* (33.30 ± 8.30 μg ml^{-1}) and *E. coli* (41.70 ± 8.30 μg ml^{-1}), as mentioned in Table 1.

3.5. Thermodynamic study

The four panels in Fig. 4 show the dependence of absorbance as a function at the CuNP concentration for different bacterial cultures, according to Table 2. The results indicate that the absorbance exponentially decays according to [**Equation 8**]. From absorbance curves, we can directly extract the baseline absorbance A_0 and k proportionality factor related to the Gibbs free energy change by a linear fit in a log-log scale (Table 2). It is important to note that when the concentration of CuNPs is higher than 100 μg ml^{-1}, the baseline absorbance A_0 trend to extreme values A_0 = 0.52 for *S. aureus* and A_0 = 1.66 for *B. subtilis*. This result could be due to *S. aureus* and *B. subtilis* containing dissimilar biosynthetic genes. In an earlier report, *in vitro* reconstitution shows that the pathways for cell wall teichoic acid biosynthesis in *B. subtilis* W23 and *S. aureus* are different. *S. aureus* required glycerol-phosphate primase called TarF to make RboP-WTAs while *B. subtilis* W23 contains a TarF homolog, but this enzyme makes glycerol-phosphate polymers and is not involved in RboP-WTA synthesis [38]. Focusing on k/RT, the values are constant and related.

Table 1
Minimum inhibitory concentration (MIC) and Maximum biocidal concentration (MBC) of CuNPs in μg ml^{-1} for four different bacterial strains (indicating the mean value and standard error of each experiment).

Microorganism	MIC (μg ml^{-1})	MBC (μg ml^{-1})
Salmonella typhi	33.30 ± 8.30	125.00 ± 0.00
Escherichia coli	41.70 ± 8.30	100.00 ± 14.40
Staphylococcus aureus	66.70 ± 8.30	116.70 ± 8.30
Bacillus subtilis	58.30 ± 8.30	108.30 ± 8.30

4. Discussion

SEM and AFM results revealed the compact, regular structural nature of CPs that may result in suitable viscosifying properties [39]. Microbial biopolymers with added viscosifying properties are already reported for good stabilization and synthesis of metal NPs [40]. In our study, the stable exothermic effect at a temperature of 246.39°C with an exact degradation temperature (T_d) of ~283.10°C shows steady thermal degradation of CPs with increasing temperature. This result concludes the thermal stability of CPs leading to prospective industrial use. Elemental analysis through the EDS spectrum indicates that the cell wall biopolymer used in our study is mainly carbonated in structure.

Non-essential metals like silver or essential metals like copper can be lethal at deficient concentrations to the bacteria [41]. Hence, in this study, the focus was on seeing the CuNPs for their antimicrobial activity. For CuNP synthesis, bacterial CPs were used as a precursor and $CuSO_4$ solution as a substrate. Based on the quantity of synthesized nanoparticles, the 1:1 (w/w) ratio of precursor and substrate was considered the best synthesis condition. Among characteristic features, SPR is vital to determine the size and shape of NPs, their inter-particle distances, and the nature of synthesized NPs [35,42]. Photoluminescence spectra of the CPs-mediated CuNPs showed decreased intensity at the time of NP production compared to the control $CuSO_4$ solution, confirming the formation of NPs. Emission bands around 610 nm (E_{max}) with a low-intensity peak of 500 nm (Fig. 2C–2E) are the characteristic peaks of CuNP, which was also earlier reported for a chemically modified chitosan biopolymer matrix [43]. Stable emission bands, intensity peaks, and the absence of sub-peaks primarily confirmed

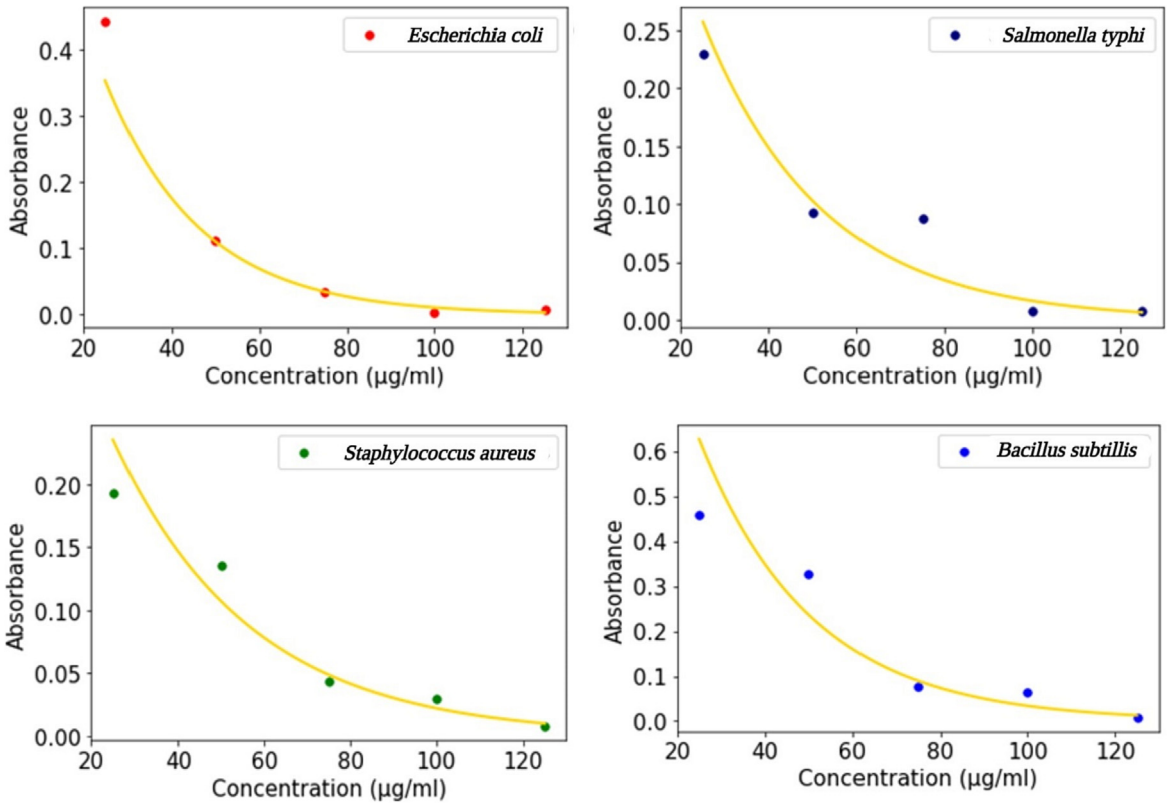

Fig. 4. Thermodynamics study showing absorbance as a function at the CuNPs concentration for different bacterial strains.

Table 2
Values of the baseline absorbance A_0 and k/RT proportionality factor related to the Gibbs free energy change (See [**Equation 8**] for CuNPs in μg ml^{-1} for four different bacterial strains.

Bacterial strain	CuNP concentration (μg ml^{-1})					A_0	k/RT	R^2
	25	50	75	100	125			
Salmonella typhi	0.230	0.092	0.087	0.008	0.008	0.64	0.04	0.88
Escherichia coli	0.442	0.113	0.035	0.004	0.007	1.13	0.05	0.90
Staphylococcus aureus	0.193	0.135	0.044	0.030	0.008	0.52	0.03	0.96
Bacillus subtilis	0.458	0.327	0.075	0.063	0.008	1.66	0.04	0.92

the synthesis of CuNPs [35]. From the FTIR spectrum, the modification of functional groups of CPs after the synthesis of CuNP can be understood. A similar kind of result on the green synthesis of CuNP was reported previously by Hasheminya and Dehghannya [44]. The 490-530 cm^{-1} peaks showed stretching corresponding to metal-oxygen or CuNP vibration that supports the presence of the monoclinic phase of CuO NPs. Like our study, another significant peak at a range of 3500–3400 cm^{-1} for CuNP was found in a previous study by Betancourt-Galindo et al. [45]. The results obtained from FTIR studies indicate that the polysaccharides probably act as a stabilizing agent, thus preventing agglomeration of the synthesized nanoparticles [35]. The EDS analysis has confirmed the presence of both Cu and CuO in NP suspension, which endorses the reduction of Cu^{2+} to Cu (0) in the reaction mixture, as found earlier by Kannan et al. [46]. From a morphological aspect, agglomerated CuNPs were spherical, clustered, and scattered with a rough surface elementally composed of carbon>copper>oxygen>sulfur. This result indicates the presence of carbon (44.21%), probably sourced from polysaccharide's carbon backbone in the biosynthesized CuNPs [14]. The apparent existence of elemental Cu (7.60% of total weight) may be due to the crystalline nature, reported previously by Kannan et al. [46]. The magnitude (-30mV to +30mV) of zeta potential define the stability of nanoparticle colloidal suspension [27]. Electrostatic repulsion makes nanoparticles with negative zeta potential stable [36]. The zeta potential of our studied CPs-based CuNP was found to be −3.84 mV, which means the synthesized CuNP has a high repulsive force due to low negative charges on the surface. The largest agglomerate is formed in a model NP system at its isoelectric point (zeta potential = 0 mV). The further the zeta potential deviates from 0 mV, the less the particle shows agglomeration tendency due to increasing repulsive forces [47]. Such repulsion may prevent the agglomeration of NPs in solution, leading to their long-term stability. It can also regulate the *in vivo* interaction of NPs with the bacterial cell membrane. Like our studied CuNP (Z-average diameter value of 702.95 nm), a similar kind of Z-average diameter of more than 100 nm (122.7 nm) was found in the case of CuNPs synthesized previously by Patel et al. [48] using *Ocimum sanctum* plant leaf extract. In another study by Birch and Schiffman [49] on chitosan-pectin NPs, the Z-average diameter was found to vary from 400 to 700 nm in different pH (3.5–5.5). Like our studied CuNP, in another report, starch-encapsulated silver nanoparticles of 115.2 nm had shown antimicrobial activity through bacterial cell damage can have probable application in the food industry [50]. The polydispersity index (PDI) of synthesized CuNPs was 0.437 (Fig. 3E), indicating that the nanoparticles were mainly polydisperse.

From the experiments, it has been perceived that CuNP1 [CuSO4: CPs (1:1)] has optimum antibacterial activity against Gram-negative *S. typhi* and *E. coli* in contrast to CuNP2 [CuSO4: CPs (2:1)], while CuNP3 [CuSO4: CPs (1:2)] exhibit no antibacterial activity. The MIC/ MBC analysis results also clearly indicate the preferential activity of the CuNPs toward gram-negative bacteria. The high MIC/MBC values of the CuNPs against gram-negative bacteria hint at non-effective killing. Such differential activity can be attributed to the cell wall composition of Gram-positive bacteria. This type of preferential CuNP activity is also reported by Padil and Černík [51]. The plausible reason may be that Gram-negative bacteria have a thinner peptidoglycan layer compared to the Gram-positive one, making it harder for CuNPs to penetrate the cell membrane, resulting in a low antibacterial response. $CuSO_4$ is known as a traditional inorganic antibacterial material. CuNPs release Cu^{2+} ions in the liquid medium, which may be allowed by gram-negative bacteria to reach the plasma membrane and inhibit the growth of bacteria [52]. In addition, probably, the toxicity of Cu^{2+} results in rapid DNA degradation, followed by decreased bacterial respiration. It was studied before by Amer and Awwad [53] that Cu^{2+} inhibits specific cytochromes in the bacterial membrane. According to other reports, not only the structure of bacterial cell wall but also other factors like conditions used for synthesis (temperature), reaction conditions (degree of contact with organisms) or characteristic features (particle size) are responsible for the differential sensitivity toward a particular group of bacteria [54]. According to a previous report, biofabricated AgNPs differently targeted Gram-positive bacteria depending on cell surface charge [25]. The results of the present study also reveal that CuNPs are synthesized stably in a one-step greener approach using bacterial CPs that have shown efficient antibacterial behavior compared to standard drugs. *B. anthracis* cell wall is composed of Gal, ManNAc, and GlcNAc, either in a 3:1:2 ratio or in a 10:3:1 ratio with the help of α-1-6 or β-1-4 linkage. Specific cell wall carbohydrates of *B. anthracis* are responsible for pathogenicity [55]. However, in this study, the isolated strain was already reported earlier to be non-pathogenic [56]. Therefore, the polysaccharides isolated from the bacteria can be used as future drug resources.

5. Conclusions

In this present study, we have used CPs (isolated from hot spring-origin bacteria *B. anthracis* PFAB2) as a capping and stabilizing agent for the synthesis of CuNPs through a green approach. NPs are found to be moderately monodisperse with moderate stability in an aqueous solution. However, the CPs itself have no antibacterial properties. Still, the biosynthesized CuNPs have shown elevated bactericidal properties against gram-negative *S. typhi* and *E. coli,* along with other Gram-positive bacteria. We know that bacterial CPs as biopolymers are little explored compared to bacterial EPSs. Thus, this study may open a new path for future studies to treat harmful microorganisms resistant to traditional antibiotics in a green way. However, further experiments are needed to study the efficacy of a broader range of microorganisms to establish their antimicrobial property successfully.

Author contributions

-Study conception and design: R Bandopadhyay
-Data collection: A Banerjee, RK Roy, JL López, S Vuree
-Analysis and interpretation of results: A Banerjee, S Sarkar, JL López
-Draft manuscript preparation: A Banerjee, S Sarkar, JL López

-Revision of the results and approval of the final version of the manuscript: A Banerjee, RK Roy, S Sarkar, JL López, S Vuree, R Bandopadhyay

Financial support

Concurso de Fomento a la Vinculación Internacional para Instituciones de Investigación FOVI220149, and Fondecy Regular 1231917 project by the Government of Chile.

Conflicts of interest

The authors declare no conflict of interest.

Acknowledgments

R.K.R. and R.B. are thankful to DST FIST (No. SR/FST/LS-1/2018/188(C), Department of Botany, The University of Burdwan for instrumentation facility. All the authors are also thankful to Mrs. Lisa Banerjee for providing language assistance.

Supplementary material

https://doi.org/10.1016/j.ejbt.2023.11.005.

References

[1] Banerjee A, Halder U, Bandopadhyay R. Preparations and applications of polysaccharide based green synthesized metal nanoparticles: A state-of-the-art. J Clust Sci 2017;28:1803–13. https://doi.org/10.1007/s10876-017-1219-8.
[2] Sathiyanarayanan G, Dineshkumar K, Yang YH. Microbial exopolysaccharide-mediated synthesis and stabilization of metal nanoparticles. Crit Rev Microbiol 2017;43(6):731–52. https://doi.org/10.1080/1040841X.2017.1306689. PMid: 28440091.
[3] Liu J, Qin G, Raveendran P, et al. Facile "green" synthesis, characterization, and catalytic function of β-D-glucose-stabilized Au nanocrystals. Chem–A Eur J 2006;12(8):2131–8. https://doi.org/10.1002/chem.200500925. PMid: 16358347.
[4] Balantrapu K, Goia DV. Silver nanoparticles for printable electronics and biological applications. J Mater Res 2009;24(9):2828–36. https://doi.org/10.1557/jmr.2009.0336.
[5] Vollmer W, Bertsche U. Murein (peptidoglycan) structure, architecture and biosynthesis in *Escherichia coli*. Biochimica et Biophysica Acta (BBA)-Biomembranes 2008;1778(9):1714–34. https://doi.org/10.1016/j.bbamem.2007.06.007. PMid: 17658458.
[6] Turner RD, Mesnage S, Hobbs JK, et al. Molecular imaging of glycan chains couples cell-wall polysaccharide architecture to bacterial cell morphology. Nat Commun 2018;9(1):1263. https://doi.org/10.1038/s41467-018-03551-y. PMid: 29593214.
[7] Arendsen LP, Thakar R, Sultan AH. The use of copper as an antimicrobial agent in health care, including obstetrics and gynecology. Clin Microbiol Rev 2019;32(4):e00125–e218. https://doi.org/10.1128/CMR.00125-18. PMid: 31413046.
[8] Chatterjee AK, Sarkar RK, Chattopadhyay AP, et al. A simple robust method for synthesis of metallic copper nanoparticles of high antibacterial potency against *E. coli*. Nanotechnology 2012;23(8):085103. https://doi.org/10.1088/0957-4484/23/8/085103. PMid: 22293320.
[9] Cho KH, Park JE, Osaka T, et al. The study of antimicrobial activity and preservative effects of nanosilver ingredient. Electrochim Acta 2005;51(5):956–60. https://doi.org/10.1016/j.electacta.2005.04.071.
[10] Jung WK, Koo HC, Kim KW, et al. Antibacterial activity and mechanism of action of the silver ion in *Staphylococcus aureus* and *Escherichia coli*. Appl Environ Microbiol 2008;74(7):2171–8. https://doi.org/10.1128/AEM.02001-07. PMid: 18245232.
[11] Durán N, Marcato PD, De Souza GI, et al. Antibacterial effect of silver nanoparticles produced by fungal process on textile fabrics and their effluent treatment. J Biomed Nanotechnol 2007;3(2):203–8. https://doi.org/10.1166/jbn.2007.022.
[12] Manjari G, Saran S, Arun T, et al. Facile *Aglaia elaeagnoidea* mediated synthesis of silver and gold nanoparticles: Antioxidant and catalysis properties. J Clust Sci 2017;28:2041–56. https://doi.org/10.1007/s10876-017-1199-8.
[13] Sarkar S, Ponce NT, Banerjee A, et al. Green polymeric nanomaterials for the photocatalytic degradation of dyes: A review. Environ Chem Lett 2020;18:1569–80. https://doi.org/10.1007/s10311-020-01021-w. PMid: 32837482.
[14] Rajoka MSR, Mehwish HM, Zhang H, et al. Antibacterial and antioxidant activity of exopolysaccharide mediated silver nanoparticle synthesized by *Lactobacillus brevis* isolated from Chinese koumiss. Colloids Surf B Biointerfaces 2020;186:110734. https://doi.org/10.1016/j.colsurfb.2019.110734. PMid: 31865119.
[15] Ruparelia JP, Chatterjee AK, Duttagupta SP, et al. Strain specificity in antimicrobial activity of silver and copper nanoparticles. Acta Biomater 2008;4(3):707–16. https://doi.org/10.1016/j.actbio.2007.11.006. PMid: 18248860.
[16] Gopalakrishnan V, Muniraj S. Neem flower extract assisted green synthesis of copper nanoparticles–optimisation, characterisation and anti-bacterial study. Mater Today: Proc 2021;36:832–6. https://doi.org/10.1016/j.matpr.2020.07.013.
[17] Wang L, Hu C, Shao L. The antimicrobial activity of nanoparticles: Present situation and prospects for the future. Int J Nanomed 2017;12:1227. https://doi.org/10.2147/IJN.S121956. PMid: 28243086.
[18] Usha R, Prabu E, Palaniswamy M, et al. Synthesis of metal oxide nano particles by *Streptomyces* sp. for development of antimicrobial textiles. Global J Biotechnol Biochem 2010;5(3):153–60.
[19] Singh AV, Patil R, Anand A, et al. Biological synthesis of copper oxide nano particles using *Escherichia coli*. Curr Nanosci 2010;6(4):365–9. https://doi.org/10.2174/157341310791659062.
[20] Mukherjee P. *Stenotrophomonas* and *Microbacterium*: Mediated biogenesis of copper, silver and iron nanoparticles—Proteomic insights and antibacterial properties versus biofilm formation. J Clust Sci 2017;28:331–58. https://doi.org/10.1007/s10876-016-1097-5.
[21] Brandão IYDNV, de Macedo EF, de Souza Silva PHB, et al. Bionanomining of copper-based nanoparticles using pre-processed mine tailings as the precursor. J Environ Manage 2023;338:117804–12. https://doi.org/10.1016/j.jenvman.2023.117804. PMid: 36996570.
[22] Borkow G, Gabbay J, Dardik R, et al. Molecular mechanisms of enhanced wound healing by copper oxide-impregnated dressings. Wound Repair Regen 2010;18(2):266–75. https://doi.org/10.1111/j.1524-475X.2010.00573.x. PMid: 20409151.
[23] Borkow G, Zatcoff RC, Gabbay J. Reducing the risk of skin pathologies in diabetics by using copper impregnated socks. Med Hypotheses 2009;73(6):883–6. https://doi.org/10.1016/j.mehy.2009.02.050. PMid: 19559540.
[24] Banerjee A, Halder U, Chaudhry V, et al. Draft genome sequence of the nonpathogenic, thermotolerant, and exopolysaccharide-producing *Bacillus anthracis* strain PFAB2 from Panifala hot water spring in West Bengal, India. Genome Announcements 2016;4(6):e01346–e1416. https://doi.org/10.1128/genomeA.01346-16. PMid: 28007848.
[25] Banerjee A, Rudra SG, Mazumder K, et al. Structural and functional properties of exopolysaccharide excreted by a novel *Bacillus anthracis* (Strain PFAB2) of hot spring origin. Indian J Microbiol 2018;58:39–50. https://doi.org/10.1007/s12088-017-0699-4. PMid: 29434396.
[26] Mandal D, Dash SK, Das B, et al. Bio-fabricated silver nanoparticles preferentially targets Gram positive depending on cell surface charge. Biomed Pharmacother 2016;83:548–58. https://doi.org/10.1016/j.biopha.2016.07.011. PMid: 27449536.
[27] Banerjee A, Das D, Rudra SG, et al. Characterization of exopolysaccharide produced by *Pseudomonas* sp. PFAB4 for synthesis of EPS-coated AgNPs with antimicrobial properties. J Polym Environ 2020;28:242–56. https://doi.org/10.1007/s10924-019-01602-z.
[28] Laiman V, Heriyanto DS, Lee YL, et al. Zinc oxide nanoparticles promote YAP/TAZ nuclear localization in alveolar epithelial type II cells. Atmos 2022;13(2):334. https://doi.org/10.3390/atmos13020334.
[29] Adhikari S, Lohar S, Kumari B, et al. Cu (II) complex of a new isoindole derivative: Structure, catecholase like activity, antimicrobial properties and bio-molecular interactions. New J Chem 2016;40(12):10094–9. https://doi.org/10.1039/C6NJ02193J.
[30] Nagpal UM, Bankar AV, Pawar NJ, et al. Equilibrium and kinetic studies on biosorption of heavy metals by leaf powder of paper mulberry (*Broussonetia papyrifera*). Water Air Soil Pollut 2011;215:177–88. https://doi.org/10.1007/s11270-010-0468-z.
[31] Li YH, Di Z, Ding J, et al. Adsorption thermodynamic, kinetic and desorption studies of Pb^{2+} on carbon nanotubes. Water Res 2005;39(4):605–9. https://doi.org/10.1016/j.watres.2004.11.004. PMid: 15707633.
[32] Nayak A, Sahoo JK, Sahoo SK, et al. Removal of Congo red dye from aqueous solution using zinc oxide nanoparticles synthesised from *Ocimum sanctum* (Tulsi leaf): A green approach. Int J Environ Anal Chem 2022;102(19):7889–910. https://doi.org/10.1080/03067319.2020.1842386.
[33] Ali Fil B, Korkmaz M, Özmetin G. An empirical model for adsorption thermodynamics of copper (II) from solutions onto illite clay-batch process design. J Chil Chem Soc 2014;59(4):2686–91. https://doi.org/10.4067/S0717-97072014000400012.
[34] Wu J, Xia A, Chen C, et al. Adsorption thermodynamics and dynamics of three typical dyes onto bio-adsorbent spent substrate of *Pleurotus eryngii*. Int J Environ Res Public Health 2019;16(5):679. https://doi.org/10.3390/ijerph16050679. PMid: 30813535.
[35] Rehana D, Mahendiran D, Kumar RS, et al. Evaluation of antioxidant and anticancer activity of copper oxide nanoparticles synthesized using medicinally important plant extracts. Biomed Pharmacother 2017;89:1067–77. https://doi.org/10.1016/j.biopha.2017.02.101. PMid: 28292015.
[36] Paszkiewicz M, Gołąbiewska A, Rajski Ł, et al. Synthesis and characterization of monometallic (Ag, Cu) and bimetallic Ag-Cu particles for antibacterial and

antifungal applications. J Nanomater 2016;2016(5):2187940. https://doi.org/10.1155/2016/2187940.
[37] Pal P, Banerjee A, Soren K, et al. Novel biocide based on cationic derivative of psyllium: Surface modification and antibacterial activity. J Polym Environ 2019;27(6):1178–90. https://doi.org/10.1007/s10924-019-01419-w.
[38] Brown S, Meredith T, Swoboda J, et al. *Staphylococcus aureus* and *Bacillus subtilis* W23 make polyribitol wall teichoic acids using different enzymatic pathways. Chem Biol 2010;17(10):1101–10. https://doi.org/10.1016/j.chembiol.2010.07.017. PMid: 21035733.
[39] Sajna KV, Sukumaran RK, Gottumukkala LD, et al. Studies on structural and physical characteristics of a novel exopolysaccharide from *Pseudozyma* sp. NII 08165. Int J Biol Macromol 2013;59:84–9. https://doi.org/10.1016/j.ijbiomac.2013.04.025. PMid: 23597707.
[40] Mokhtarzadeh A, Alibakhshi A, Hejazi M, et al. Bacterial-derived biopolymers: Advanced natural nanomaterials for drug delivery and tissue engineering. TrAC Trends Anal Chem 2016;82:367–84. https://doi.org/10.1016/j.trac.2016.06.013.
[41] Palza H. Antimicrobial polymers with metal nanoparticles. Int J Mol Sci 2015;16(1):2099–116. https://doi.org/10.3390/ijms16012099. PMid: 25607734.
[42] Jain PK, Huang X, El-Sayed IH, et al. Review of some interesting surface plasmon resonance-enhanced properties of noble metal nanoparticles and their applications to biosystems. Plasmonics 2007;2:107–18. https://doi.org/10.1007/s11468-007-9031-1.
[43] Tiwari AD, Mishra AK, Mishra SB, et al. Stabilisation of silver and copper nanoparticles in a chemically modified chitosan matrix. Carbohydr Polym 2013;92(2):1402–7. https://doi.org/10.1016/j.carbpol.2012.10.008. PMid: 23399170.
[44] Hasheminya SM, Dehghannya J. Green synthesis and characterization of copper nanoparticles using *Eryngium caucasicum* Trautv aqueous extracts and its antioxidant and antimicrobial properties. Part Sci Technol 2020;38(8):1019–26. https://doi.org/10.1080/02726351.2019.1658664.
[45] Betancourt-Galindo R, Reyes-Rodriguez PY, Puente-Urbina BA, et al. Synthesis of copper nanoparticles by thermal decomposition and their antimicrobial properties. J Nanomater 2014;2014:. https://doi.org/10.1155/2014/980545980545.
[46] Kannan S, Solomon A, Krishnamoorthy G, et al. Liposome encapsulated surfactant abetted copper nanoparticles alleviates biofilm mediated virulence in pathogenic *Pseudomonas aeruginosa* and MRSA. Sci Rep 2021;11(1):1102. https://doi.org/10.1038/s41598-020-79976-7.
[47] Berg JM, Romoser A, Banerjee N, et al. The relationship between pH and zeta potential of ~30 nm metal oxide nanoparticle suspensions relevant to in vitro toxicological evaluations. Nanotoxicology 2009;3:276–83. https://doi.org/10.3109/17435390903276941.
[48] Patel BH, Channiwala MZ, Chaudhari SB, et al. Biosynthesis of copper nanoparticles; its characterization and efficacy against human pathogenic bacterium. J Environ Chem Eng 2016;4(2):2163–9. https://doi.org/10.1016/j.jece.2016.03.046.
[49] Birch NP, Schiffman JD. Characterization of self-assembled polyelectrolyte complex nanoparticles formed from chitosan and pectin. Langmuir 2014;30(12):3441–7. https://doi.org/10.1021/la500491c. PMid: 24593694.
[50] Saravanakumar K, Sriram B, Sathiyaseelan A, et al. Synthesis, characterization, and cytotoxicity of starch-encapsulated biogenic silver nanoparticle and its improved anti-bacterial activity. Int J Biol Macromol 2021;182:1409–18. https://doi.org/10.1016/j.ijbiomac.2021.05.036. PMid: 33965484.
[51] Padil VVT, Černík M. Green synthesis of copper oxide nanoparticles using gum karaya as a biotemplate and their antibacterial application. Int J Nanomed 2013;8(1):889–98. https://doi.org/10.2147/IJN.S40599. PMid: 2346739752.
[52] Raffi M, Mehrwan S, Bhatti TM, et al. Investigations into the antibacterial behavior of copper nanoparticles against *Escherichia coli*. Ann Microbiol 2010;60(1):75–80. https://doi.org/10.1007/s13213-010-0015-6.
[53] Amer M, Awwad A. Green synthesis of copper nanoparticles by Citrus limon fruits extract, characterization and antibacterial activity. Chem Int 2021;7(1):1–8.
[54] Liang X, Sun M, Li L, et al. Preparation and antibacterial activities of polyaniline/$Cu_{0.05}Zn_{0.95}O$ nanocomposites. Dalton Trans 2012;41(9):2804–11. https://doi.org/10.1039/C2DT11823H. PMid: 22249414.
[55] Choudhury B, Leoff C, Saile E, et al. The structure of the major cell wall polysaccharide of *Bacillus anthracis* is species-specific. J Biol Chem 2006;281(38):27932–41. https://doi.org/10.1074/jbc.M605768200. PMid: 16870610.
[56] Banerjee A, Somani VK, Chakraborty P, et al. Molecular and genomic characterization of PFAB2: A non-virulent *Bacillus anthracis* strain isolated from an Indian hot spring. Curr Genomics 2019;20(7):491–507. https://doi.org/10.2174/1389202920666191203121610. PMid: 32655288.